Infragravity Seiches in a Small Harbor

G. Cuomo[1] and R. T. Guza[2]

Abstract: A method is developed to estimate harbor seiche at Marina di Carrara, Italy, from the properties of wind-generated incident waves outside the harbor. A linear model of the spatial structure of amplified seiche modes is combined with empirical estimates of the response of each mode to variable incident wave forcing. These empirical coefficients parameterize the complex nonlinear transfer of energy from wind waves to lower frequency seiche. As at other small harbors (<1 km^2 surface area) on ocean coasts, and consistent with previous analyses at Carrara, the observed seiche is relatively energetic at several periods between about 1 and 15 min that are highly amplified theoretically, and the spatial structure of modeled and observed seiches agree as well. The longest seiche (≈15 min) mode is almost spatially uniform within the harbor and dominates with low-energy, short-period incident wind waves (measured 1 km offshore of the harbor). Increased wave energy and longer periods excite shorter period (1–3 min) seiche modes with more complex spatial structure, including small areas of high amplification, which have led to operational issues. The energy in each of the six most energetic seiche modes is related in this paper empirically to offshore incident wind wave height and peak period, allowing detailed predictions of harbor seiche from routine wind wave forecasts. The approach appears applicable to relatively small, shallow harbors with reflective quay walls, in which the exterior harbor mouth is exposed, and the interior sheltered from energetic wind-generated waves. **DOI: 10.1061/(ASCE)WW.1943-5460.0000392.**

Author keywords: Seiches; Harbor resonance; Infragravity waves; Field measurements.

Introduction

Harbor seiches can cause excessive vessel movements and compromise harbor operations [Seabergh (1993); Lee et al. (1998); Poon et al. (1998); Li (2002); Briggs et al. (2005); and many others]. In small coastal harbors, seiching is often excited by infragravity waves and more rarely by atmospheric pressure oscillations (Gomis et al. 1993; Vidal et al. 2000; de Jong and Battjes 2004), tsunamis (Lepelletier 1981; Lepelletier and Raichlen 1987), earthquakes (Ichinose et al. 2000), and internal waves (Graham et al. 1990). Discussed here are seiches at infragravity wave periods of a few minutes, often dominating water-level oscillations in a small area (<1 km^2), and shallow (<12 m) harbors on ocean coasts (Bowers 1992; Melito et al. 2006).

Infragravity waves are generated by nonlinear difference interactions between shorter period, wind-generated waves [Munk (1949) and many others]. The dynamics (e.g., nonlinear generation, dissipation, trapping) determining infragravity energy levels on beaches and in harbors are understood incompletely and cannot yet be accurately predicted theoretically. Time-dependent nonlinear Boussinesq models of harbor seiche are promising, but still in development (Woo and Liu 2004; Melito et al. 2007; Losada et al. 2008; Thotagamuwage and Pattiaratchi 2013; Guerrini et al. 2014).

Many authors have empirically related total (frequency-integrated) infragravity energy on beaches (Stockdon et al. 2006) and in harbors (Bowers 1992) to incident wave conditions.

Here, infragravity seiche observed in Marina di Carrara, Italy, is shown to agree well with solutions to the linear, steady-state, mild-slope equation, which is similar to previous results at Carrara (Melito et al. 2007; Guerrini et al. 2014) and other small harbors (Okihiro and Guza 1996).

A new method to estimate the time-varying (hourly) energy of individual seiche modes from harbor observations is used to empirically relate the individual mode energies to incident wind wave conditions. The estimation of the detailed space-time structure of harbor seiche from routinely available wind wave statistics is demonstrated in the final part of the paper.

Marina di Carrara: Site and Basic Observations

Marina di Carrara, a commercial harbor with limited fetch on the Mediterranean Sea, is exposed primarily to south-southwest (SSW) short wind waves [Fig. 1(a)]. The approximately square harbor has a surface area of 0.36 km^2, mean depth of 10.5 m, and a lateral entrance width of 120 m [Fig. 1(c)]. The spring tidal range (0.36 m) and typical storm surge (<0.60 m) are relatively small. The basin perimeter (total length 1650 m) consists mostly of vertical quay walls [Fig. 1(b)]. The harbor interior is well protected from the dominant southwest wind waves [Fig. 1(c)], and water level fluctuations within the harbor are dominated by seiches with infragravity periods (a few minutes) (Melito et al. 2006, 2007; Belotti and Franco 2011).

Wind-generated incident waves (WW; frequency 0.05–0.33 Hz) were monitored about 1 km offshore (13.5 m depth) with a Datawell (Haarlem, Netherlands) directional wave buoy. Infragravity waves (IG: frequency 0.0005–0.02 Hz) were observed inside the harbor using eight synchronized, continuously sampling (at

[1]Research Director, HR Wallingford Ltd., Howbery Park, Wallingford OX10 8BA, U.K. (corresponding author). E-mail: g.cuomo@hrwallingford.com

[2]Professor Emeritus, Scripps Institution of Oceanography, Univ. of California, San Diego, CA 92093-0209. E-mail: rguza@ucsd.edu

Note. This manuscript was submitted on June 16, 2016; approved on December 16, 2016; published online on July 11, 2017. Discussion period open until December 11, 2017; separate discussions must be submitted for individual papers. This paper is part of the ***Journal of Waterway, Port, Coastal, and Ocean Engineering***, © ASCE, ISSN 0733-950X.

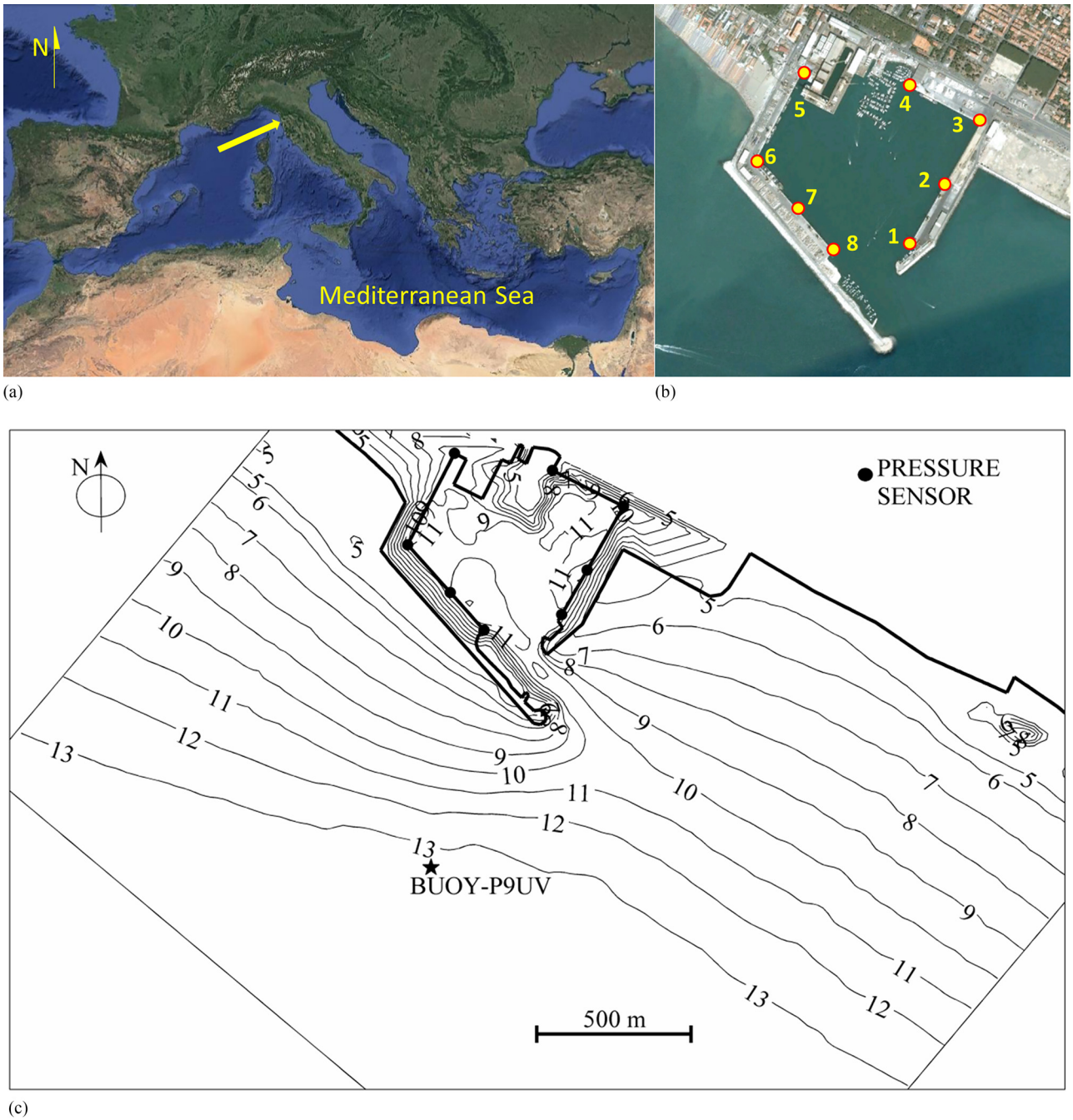

Fig. 1. Marina di Carrara Harbor, Italy: (a) geographical location and southwest arrival direction (arrow) of ocean wind waves (© Google, Imagery © 2017 Cnes/Spot Image, Digital Globe, Map data ©2017 Google); (b) aerial photograph of the harbor showing locations of pressure sensors (labeled P1–P8) along the harbor quays [© Google, Imagery ©2017 NASA, TerraMetrics, Map data ©2017 GeoBasis-DE/BKG (©2009), Google, Inst. Geogr. National, Mapa GISrael, ORION-ME]; (c) harbor and local shelf bathymetry; P9UV is located near a directional wave buoy at a 13-m depth

2 Hz) pressure sensors, at locations along the quay walls at which high seiche elevations were anticipated (Sensors 1–8) [Fig. 1(b)], and outside the harbor, in 13.5-m depth by means of a bottom-mounted collocated current meter and pressure sensor (P9UV). Observations acquired from 2005 to 2007 were processed in 1.2-h long records. Each 1.2-h record was linearly detrended and Fourier transformed. The smoothed spectra have frequency resolutions of 2.3×10^{-4}Hz. The results are not sensitive to signal processing details (e.g., Hanning windowing does not change the results significantly). Additional descriptions of the data acquisition system, instrument sampling, and wave climate are in Melito et al. (2006, 2007).

A selected 48-h period [solid curve in Fig. 2(a)] is discussed in detail later in the text because it includes low-energy and high-energy wind waves, and illustrates the seiche response to variable forcing.

Band-integrated IG energy (E_{IG}), both within and seaward of the harbor [filled and open symbols in Fig. 2(a), respectively], covaries with band-integrated wind wave energy. Similar offshore E_{IG} are estimated using P9 and UV9 [open

J. Waterway, Port, Coastal, Ocean Eng., 2017, 143(5): 04017032

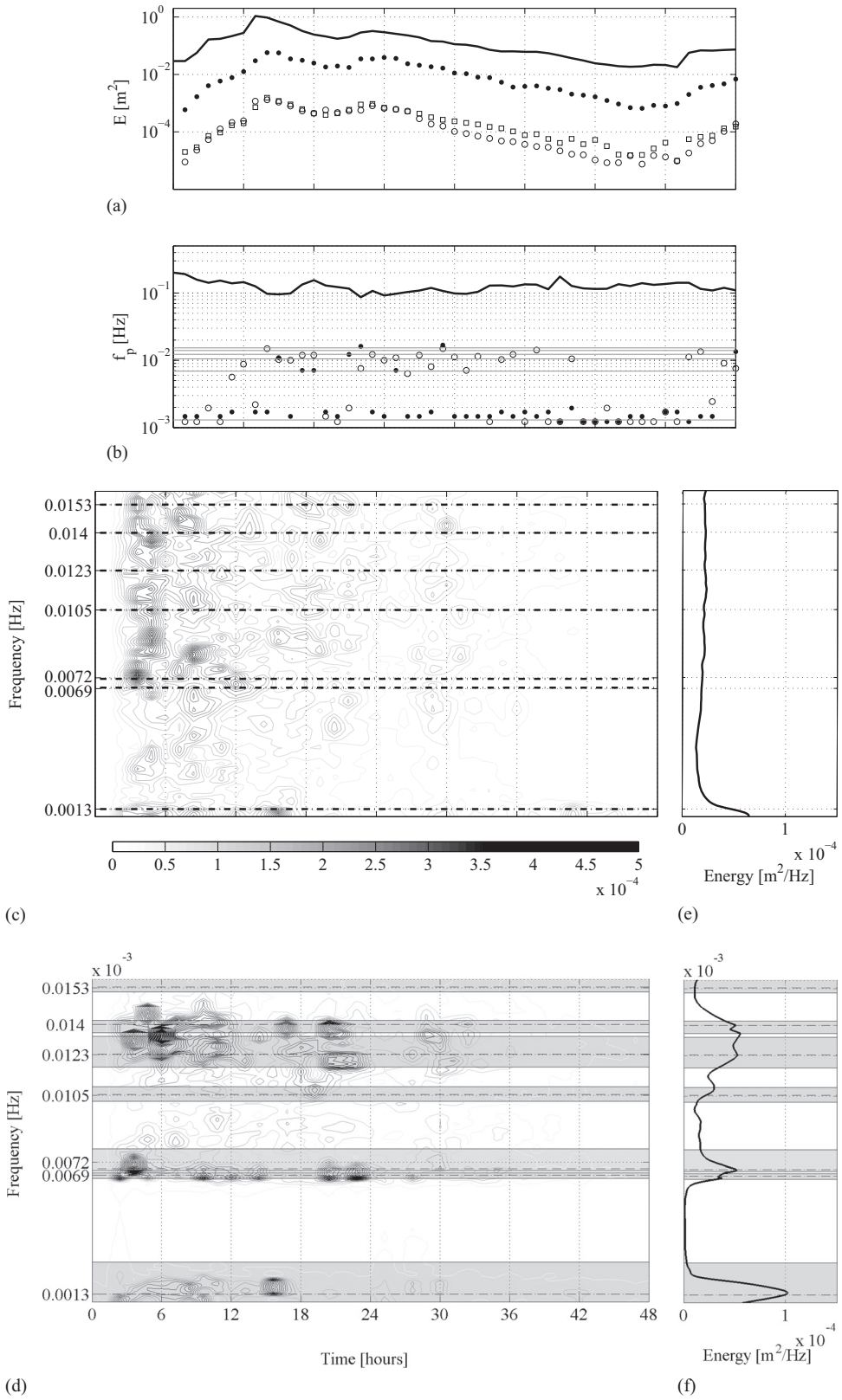

Fig. 2. (a) Wave energy E and (b) peak frequency f_p versus time for 48 typical winter hours; the solid curves are wind waves ($0.05 < f < 0.33$ Hz) in a 13.5-m depth [Note: Symbols are infragravity waves ($0.0005 < f < 0.02$ Hz), averaged over the harbor gauges P1–P8 (black circles), and outside the harbor (13.5-m depth) from velocity (UV9, open squares) and from pressure (P9, open circles)]; (c) infragravity frequency spectra $E_{IG}(f)$ seaward of the harbor (13.5-m depth) versus frequency and time [Note: See color bar for $E_{IG}(f)$ scale]; (d) same as (c) but averaged over harbor sensors (P1–P8); (e) $E_{IG}(f)$ seaward of the harbor averaged over 48 h; (f) $E_{IG}(f)$ averaged over the harbor sensors and 48 h [Note: The horizontal dashed lines in (c), (d), (e), and (f) are theoretically resonant frequencies; the gray shading in (d) and (f) corresponds to the modal assurance criterion frequency bandwidth (see text)]

symbols in Fig. 2(a)], showing that the velocity fluctuations at infragravity frequencies at that location are dominated by waves, not eddies.

The peak wind wave frequency $f_{p,\mathrm{WW}}$ at the offshore buoy varies continuously between about 0.1–0.2 Hz [solid curve in Fig. 2(b)]. The peak infragravity frequency f_{IG}^{p} falls into two bands, around 10^{-3} and 10^{-2} Hz (both within and seaward of the harbor) [filled and open circles in Fig. 2(b)].

Energy spectra at infragravity frequencies within the harbor are consistently peaked at a few frequencies, both during individual hours [Fig. 2(d)] and 48-h averaged [Fig. 2(f)]. In contrast $E_{\mathrm{IG,offshore}}$ is relatively featureless [Fig. 2(e)]. Although resonant frequencies dominate spectra within the harbor, outside the harbor amplification is relatively weak, and the average spectra are featureless. The horizontal dashed lines in Figs. 2(d and f) are frequencies at which harbor resonance occurs, according to theory, as discussed next.

Seaward of the harbor, total E_{IG} [dashed black line in Fig. 2(a)] is correlated with E_{WW}, inversely correlated with $f_{p,\mathrm{WW}}$, and is described approximately by a power law (Fig. 3)

$$E_{\mathrm{IG}} = \alpha E_{\mathrm{WW}}^{\beta} f_{p,\mathrm{WW}}^{\gamma} \tag{1}$$

The best fits $\alpha = 3 \times 10^{-6}$, $\beta = 0.9$, and $\gamma = -3.0$ are similar to values based on previous analysis at Carrara (Melito et al. 2006, 2007) and in similar depths in both the Atlantic and Pacific oceans [Bowers (1992) and others]. According to Eq. (1), the dependence of $f_{p,\mathrm{WW}}$ is strong; with the same E_{WW}, E_{IG} with swell (f_p = 0.05 Hz) is about 60 times larger than with short seas (f_p = 0.2 Hz).

Although the strong inverse dependence of E_{IG} on f_p [Eq. (1)] is qualitatively consistent with bound wave theory, the observed E_{IG} is not accurately predicted by bound wave theory, similar to previous results elsewhere in similar depths (Okihiro et al. 1992; Herbers et al. 1995). To assess this in more detail, infragravity bound wave spectra in constant, 13.5-m depth were estimated from second-order theory [Longuet-Higgins and Stewart (1960); Hasselmann (1962); Sand (1982); and others] for 1.2-h long directional buoy records analyzed using the maximum likelihood method [MLM; Isobe et al. (1984)]. Bound wave predictions $E_{\mathrm{ig,bnd}}$ are not very sensitive to the details of the directional properties of E_{WW}, as long as the waves are directionally spread (Sand 1982; Bowers 1992). When incident wave forcing $\alpha E_{\mathrm{WW}}^{\beta} f_p^{\gamma}$ is small, $E_{\mathrm{ig,bnd}} < E_{\mathrm{ig,obs}}$ (Fig. 4) is consistent with a mix of free and bound waves. For large $\alpha E_{\mathrm{WW}}^{\beta} f_p^{\gamma}$, $E_{\mathrm{ig,bnd}} \approx E_{\mathrm{ig,obs}}$ and bound waves contribute a larger fraction of the total energy (Herbers et al. 1995).

The variation in infragravity wave energy outside and inside the harbor is shown in Fig. 5 as a function [via Eq. (1)] of the incident wind wave conditions outside the harbor. With the weakest wind wave forcing, total infragravity energy (both inside and outside the harbor) are dominated by the lowest Mode 1 [0.0013 Hz in Figs. 2(d and f); circles in Fig. 5]. The increasing relative importance of high-mode, high-frequency seiches with increasing E_{WW} (triangles in Fig. 5) was reported previously at Carrara (Melito et al. 2006, 2007) and three other small harbors (Okihiro and Guza 1996).

Amplification and Phase

The theoretical and observed spatial structures of amplified modes are shown here to agree, including at locations of seiche *hot spots*.

Mild-Slope Equation

Harbor seiching was modeled with a finite-element solution (Iannotta 2002) of the two-dimensional elliptic mild-slope wave equation (Berkhoff 1976)

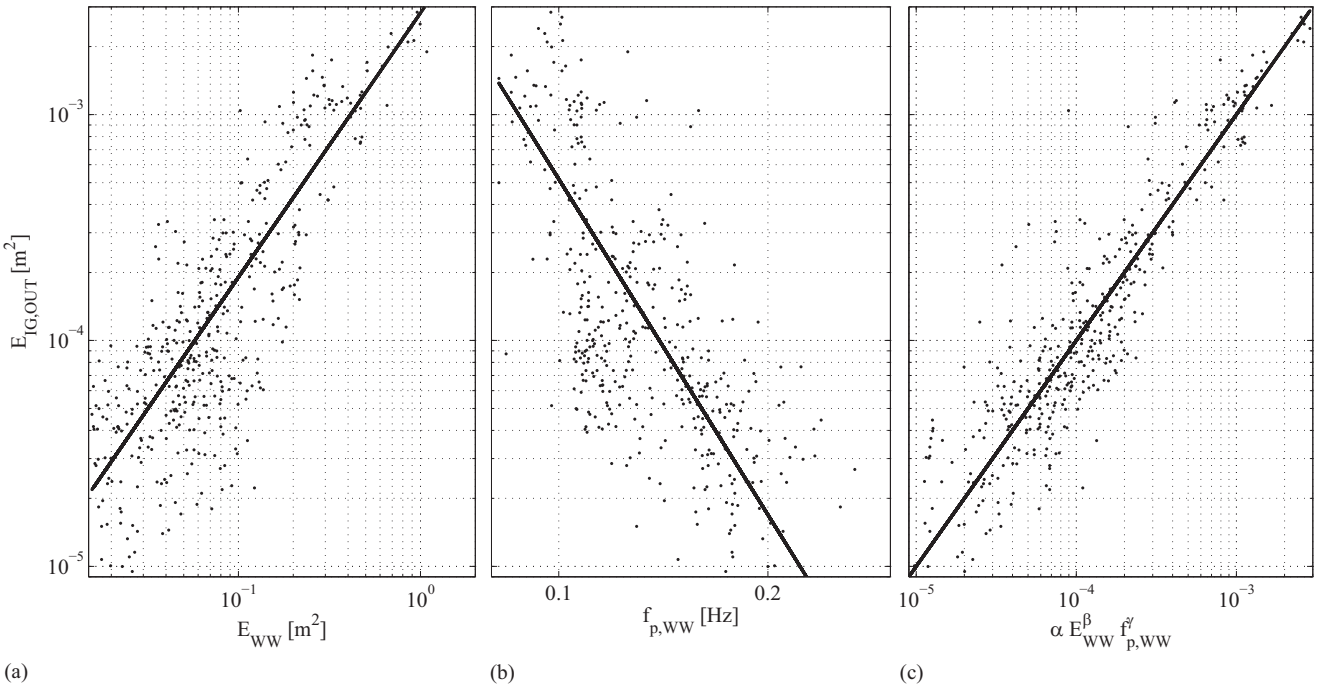

Fig. 3. Measured infragravity ($0.0005 < f < 0.003$ Hz) energy outside the harbor ($E_{\mathrm{IG,OUT}}$, 13-m depth) versus wind wave (a) energy (E_{WW}) and (b) peak frequency ($f_{p,\mathrm{WW}}$) at the collocated wave buoy (Note: The solid lines are power law fits); (c) $E_{\mathrm{IG,OUT}}$ versus $\alpha E_{\mathrm{WW}}^{\beta} f_{p,\mathrm{WW}}^{\gamma}$, with $\alpha = 3.0\ 10^{-6}$, β = 0.9, and $\gamma = 3.0$ (Note: The 1-1 line is a perfect fit; each dot is a 1.2-h record)

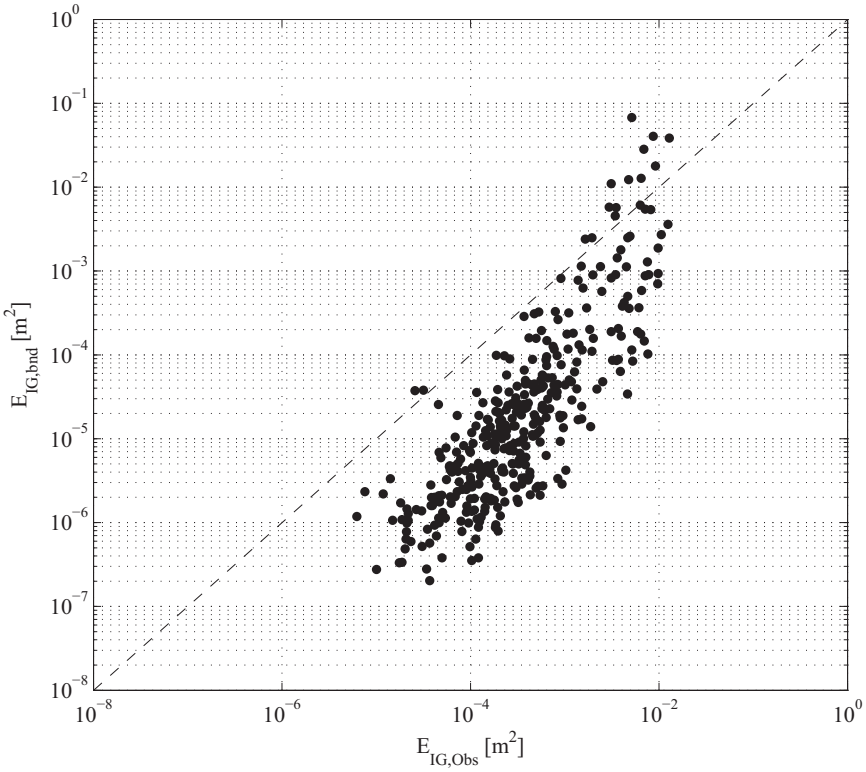

Fig. 4. Theoretically bound infragravity energy $E_{IG,bnd}$ versus observed infragravity energy $E_{IG,obs}$ in 13-m depth

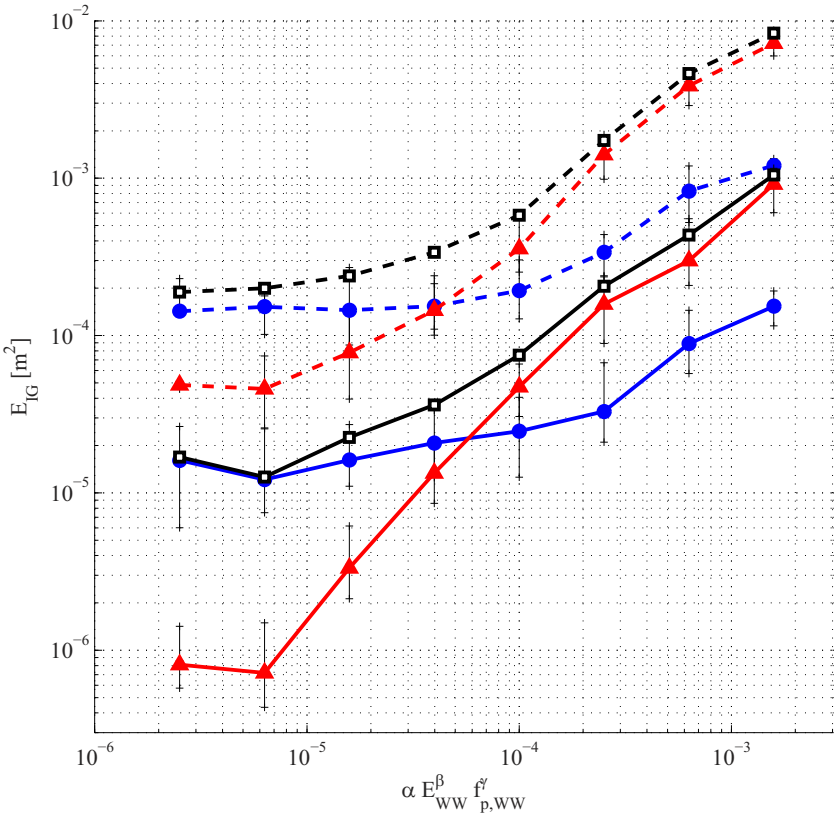

Fig. 5. Infragravity energy E_{IG} versus incident wind wave forcing; dashed curves are inside (averaged over Sensors 1–8), and solid curves are outside (P9) the harbor {Note: Vertical scatter bars indicate 1 standard deviation; wave forcing parameters α, β, and γ are best fit values for total infragravity energy outside the harbor [Fig. 7(c)]; frequency bands are low IG ($0.0005 < f < 0.00$ Hz, circles), high IG ($0.003 < f < 0.02$ Hz, triangles), and the total IG energy ($0.0005 < f < 0.02$ Hz, squares)}

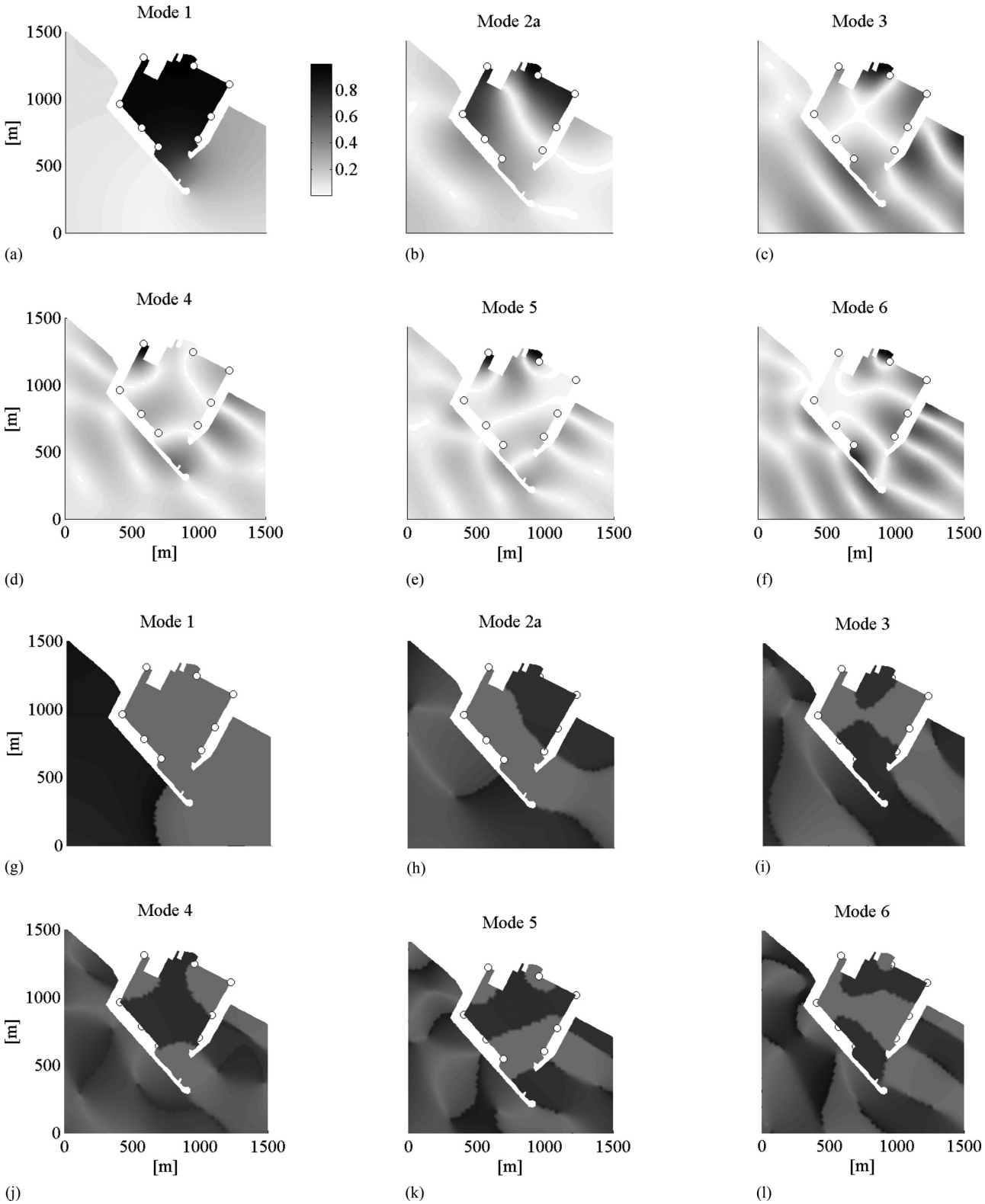

Fig. 6. (a–f) Modal amplitude and (g–l) phase for six seiche modes (frequencies in Table 1); normalized energy (see color bar) and phase (light is 0°, dark is 180°) are relative to the energy maximum in the harbor at each mode; sensor locations are in Fig. 1(b), and mode frequencies are in Table 1

$$\nabla\left(CC_g\nabla\hat{\eta}\right)+\frac{C_g}{C}\sigma^2\hat{\eta}=0 \tag{2}$$

where η = complex surface elevation; $\sigma = 2\pi f$ = angular frequency; and C and C_g = phase velocity and group velocity, respectively. The shoreline and harbor quays [bold lines in Fig. 1(c)] are assumed fully reflective (for the long waves that were simulated). Seaward boundaries were assumed totally absorptive (Steward and Panchang 2001). No attempt was made to model friction-induced losses because model results are only used in this paper to derive modal structures to inform interpretation of field observations rather than to quantify modal amplifications per se.

For each infragravity wave frequency and direction, Eq. (2) yields the (steady state) spatial variation of wave height $H(x, f)$ (equivalently energy $E(\mathbf{x},f)$) and phase $\theta(\mathbf{x},f)$.

Carrara harbor has seven amplified frequency bands between 0.0005 and 0.016 Hz [gray bands in Figs. 2(d and f)], resulting from constructive interference of reflections from the harbor walls. The spatial patterns of amplitude and phase for the amplified modes (Fig. 6) are similar to normal mode (eigen) solutions of the unforced equations, as expected for Sturm-Liouville type equations (Sobey 2006; Bellotti et al. 2012).

Results in Fig. 6 are for a long wave incident from 220°N, the same direction as the dominant wind waves. The frequencies and spatial structure of amplified modes are generally only weakly sensitive to the model long wave directions ranging between 200 and 240°N (Fig. 7). Next, the effect of variations in short and long incident wave mean directions (around the assumed SSW) are neglected.

Comparison with Observations

The theoretical spatial structure at seiche frequencies (Fig. 6) compares well with pressure sensor observations at corresponding frequencies (Fig. 8, averaged over the entire data set). Mode 1 is spatially uniform and in phase at measurement locations within the harbor and out of phase with reduced amplitude seaward of the harbor [P9, Figs. 8(a and g)]. The observed Mode 3 is amplified at Sensors 3 and 9 (outside the harbor), with the predicted complex phase structure [Figs. 8(c and i)]. Modes 4 and 5 are most strongly amplified at Sensor 5, as predicted [Figs. 8(d and e)]. Model predictions of E_{IG} outside the harbor (P9UV) are sometimes inaccurate [Sensor 9 in Figs. 8(a, b, and e)], possibly because theoretical energy levels outside the harbor are more sensitive to the incident long wave direction (assumed from the SSW) than inside the harbor. Nevertheless, modeled amplifications within the harbor relative to P9 are qualitatively correct (Fig. 9).

Estimating the Time Variation of Seiche Mode Energy

The energy in each seiche frequency band f_n, for each 1.2-h record, is estimated by minimizing the misfit Γ between the theoretical mode shape and observations

$$\Gamma(f_n)=\sum_{i=1}^{8}\left[S(\mathbf{x}_i,f_n)-E'(\mathbf{x}_i,f_n)\right]^2 \tag{3}$$

The sum is computed over all harbor Sensors P1–P8, and $S(\mathbf{x}_i,f_n)$ is the observed spectrum at sensor location $\mathbf{x}_i$. The frequency bandwidth for each mode is identified using the modal assurance criterion (MAC) (Allemang 2003), based on the similarity of spatial shapes within the band (Appendix). MAC bandwidths, shown as shaded gray bands in Figs. 2(d and f), are used in Figs. 10, 11, 12, and 13. For each frequency (f_n), $E'(\mathbf{x},f_n)$ is the theoretical spatial mode structure [Eq. (2), Appendix] with energy level $E^o_{IG,IN}(f_n)$

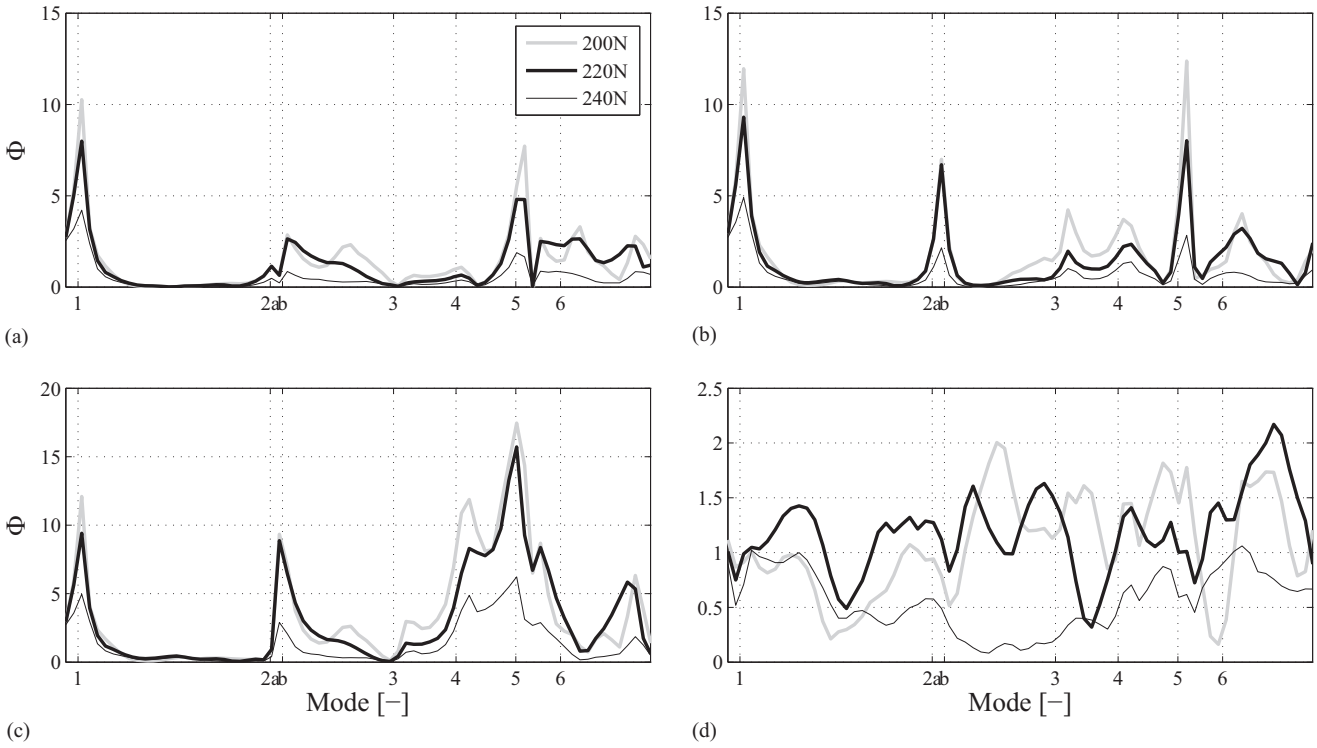

Fig. 7. Theoretical amplification (relative to the model offshore boundary) versus frequency for long wave incidence angles of 200, 220, and 240° (see legend) at Sensors (a) 1, (b) 3, (c) 5, and (d) 9UV

J. Waterway, Port, Coastal, Ocean Eng., 2017, 143(5): 04017032

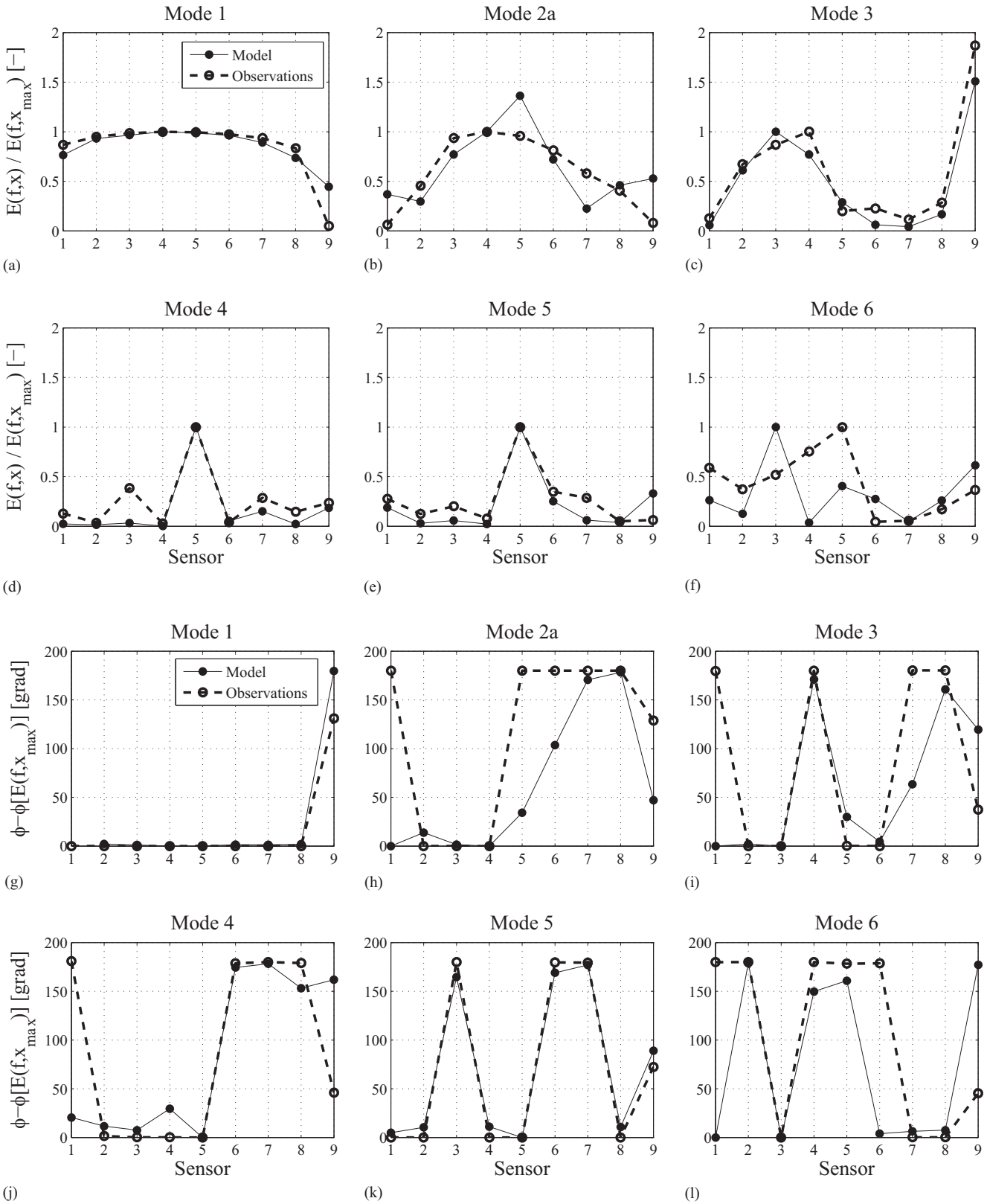

Fig. 8. (a–f) Normalized energy and (g–l) phases as observed (filled circles) and predicted by the model (open circles) for each mode, relative to the sensor with the maximum modeled amplification; sensor locations are in Fig. 1(b), and mode frequencies are in Table 1; the model and observational frequency resolution are equal, 2.3×10^{-4}Hz; results are averaged over the entire data set

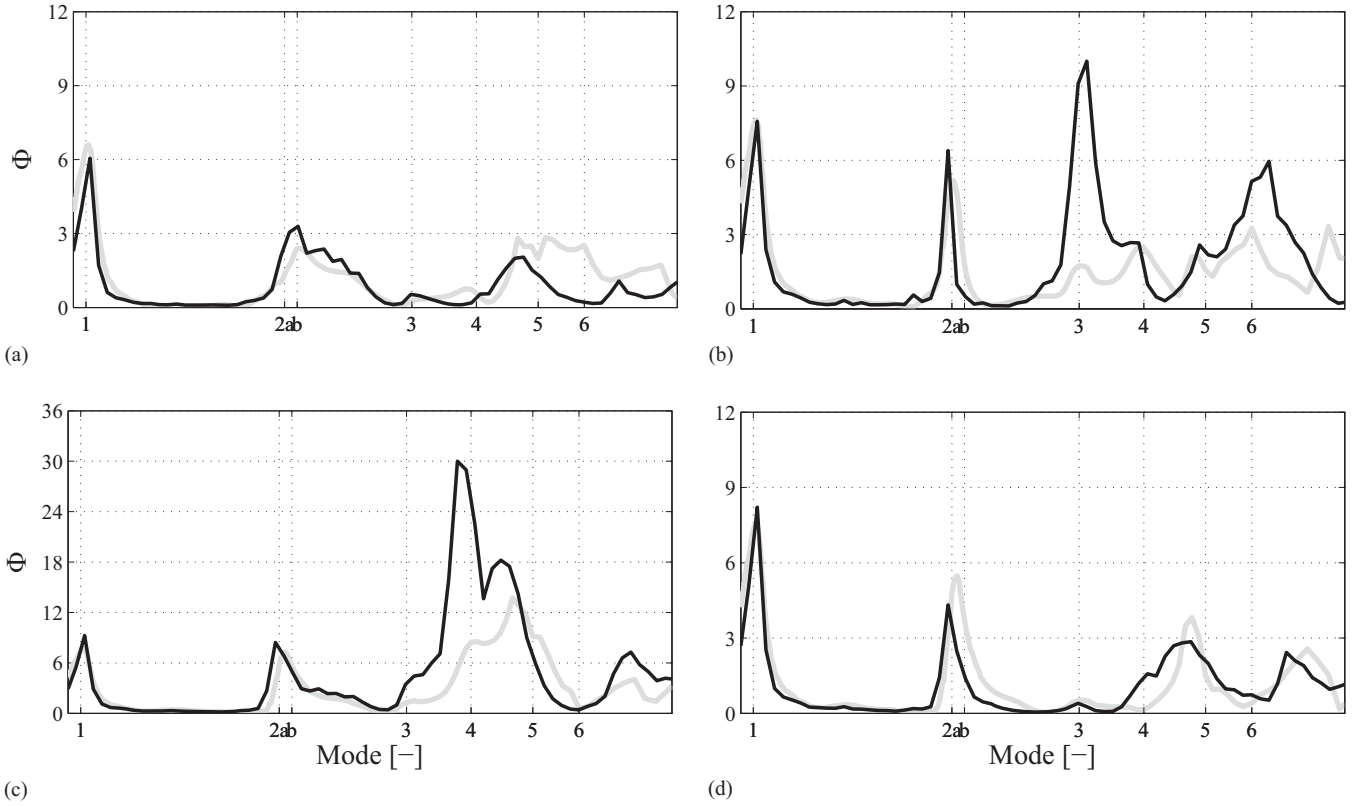

Fig. 9. Amplification diagram (Φ, energy relative to P9) versus frequency (mode numbers are indicated) at Sensors (a) 1, (b) 3, (c) 5, and (d) 6; observed diagrams (black) are averaged over all observations; the model predicted amplification (gray) is smoothed over the frequency resolution of the observations, reducing the magnitude of modeled modes that are narrower in frequency than is resolved by the observations; vertical scale of Sensor 5 is unique because Mode 4 is theoretically relatively highly amplified

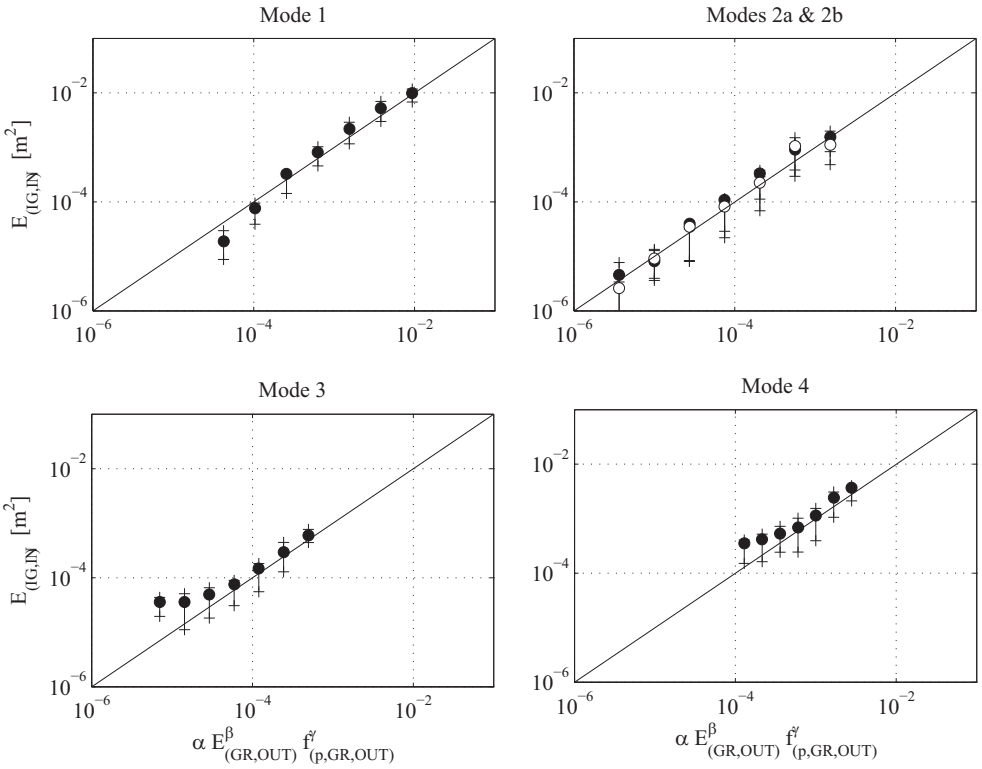

Fig. 10. Harbor infragravity mode energy $E_{IG,IN}$ (averaged over all observations) versus offshore wind wave forcing (buoy at P9); the α, β, and γ values vary between panels and are best fits for each mode; vertical bars indicate 25 and 75% quantiles

Table 1. For Each Mode Number, Frequency f, Best Fit Empirical Power Law Parameters (α, β, and γ), and MAC Bandwidth $f_{MAC,min} < df_{MAC} < f_{MAC,max}$

Mode	f (10^{-3}Hz)	α	β	γ	$f_{MAC,min}$ (10^{-3} Hz)	$f_{MAC,max}$ (10^{-3} Hz)
1	1.3	7.5×10^{-6}	0.92	–3.3	0.5	1.9
2a	6.9	5.3×10^{-8}	0.83	–4.6	6.8	7.0
2b	7.2	1.7×10^{-6}	0.96	–3.0	7.1	8.1
3	10.5	2.3×10^{-6}	0.75	–2.5	10.2	10.8
4	12.3	2.1×10^{-4}	0.65	–1.2	11.6	13.0
5	14.0	1.1×10^{-4}	0.59	–1.2	13.7	14.3
6	15.3	1.2×10^{-4}	0.60	–1.1	14.9	15.6

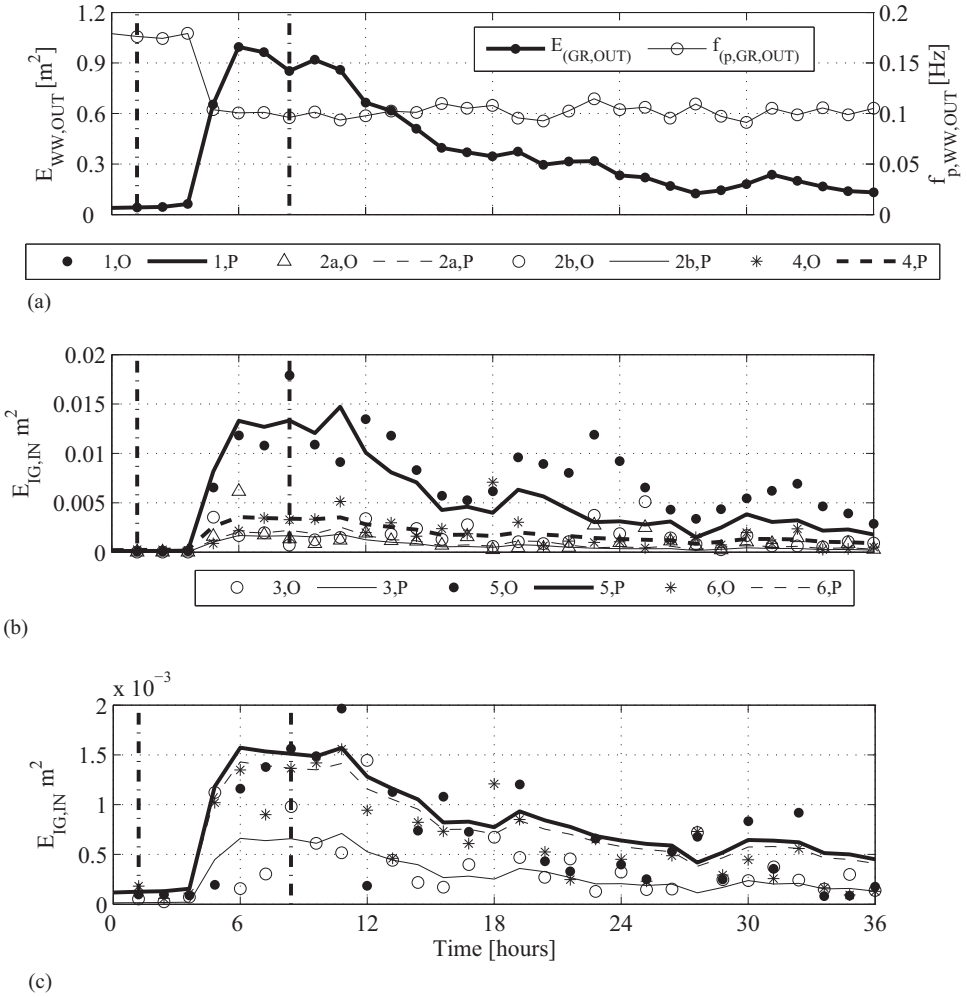

Fig. 11. (a) Wind wave energy E_{WW} and peak frequency f_p outside the harbor (left and right scales, respectively), (b and c) infragravity wave energy within the harbor in each mode observed (for symbols, see legend, O) and predicted (curves, P) versus time [Note: The vertical scales differ in (b) and (c)]

$$E'(\mathbf{x}_i, f_n) = E^o_{IG,IN}(f_n)\Psi(\mathbf{x}_i, f_n) \quad (4)$$

The shape function Ψ is normalized as

$$\sum_{i=1}^{8} \Psi(\mathbf{x}_i, f_n) = 1 \quad (5)$$

$E'(\mathbf{x}, f_n)$ is an estimate of the energy at location $\mathbf{x}$ and frequency f_n; it is independent of the locations of the calibrating sensors. The sensor locations in the present observations intentionally included theoretically highly amplified hot spots [e.g., Sensors 4 and 5 in Figs. 6(a–f)], but determination of model free parameters does not require observations at hot spots.

Empirical Relationship between Each Harbor Seiche Mode and Incident Wind Waves

Hourly observation-based estimates of $E'(\mathbf{x}, f_n)$, integrated over the MAC bandwidth for each of the seven modal f_n bands, were regressed against incident wave forcing characterized as $E_{IG} =$

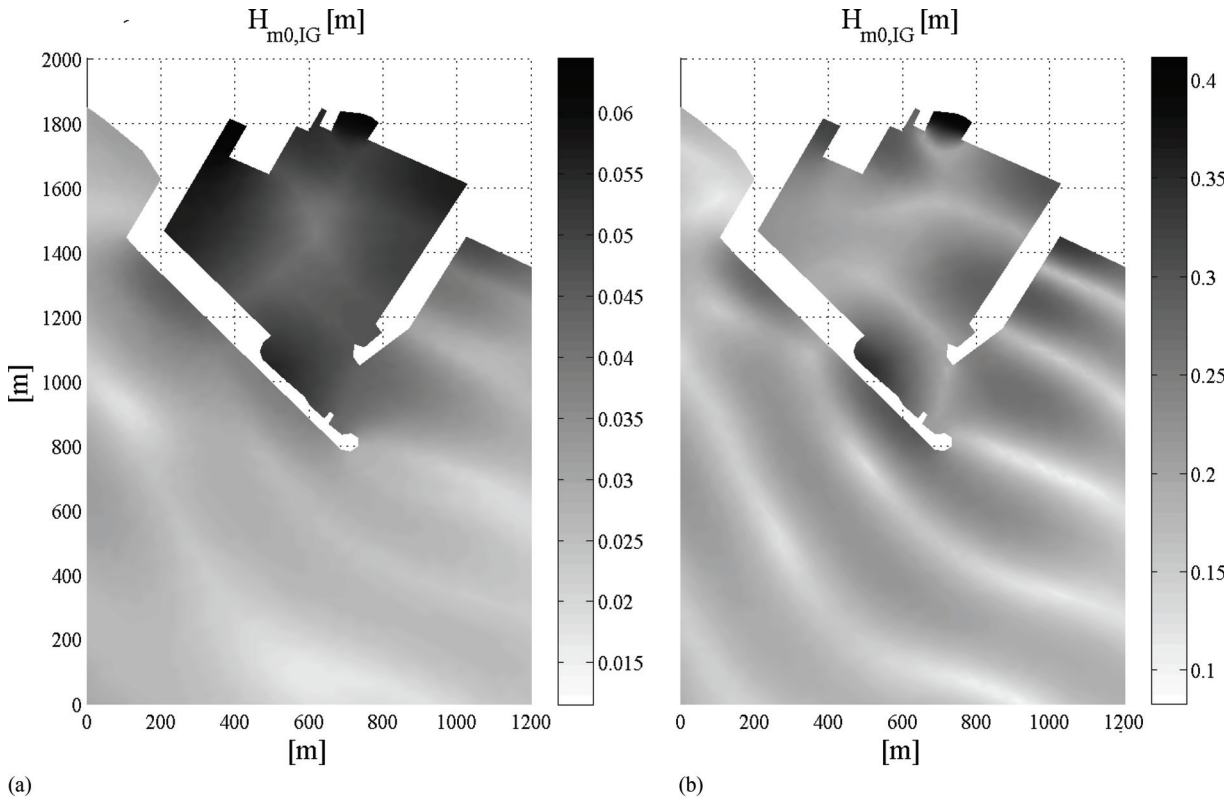

Fig. 12. Plan view of infragravity significant wave height within the harbor $H_{s,\mathrm{IG}}$ based on modal reconstructions during moderate wave conditions [$t = 1$ h, Fig. 11; $H_{m0,\mathrm{WW}} = 0.8$ m; $f_{(p,\mathrm{WW})} = 0.18$ Hz], and at the storm peak [$t = 8$ h; $H_{m0,\mathrm{WW}} = 3.7$ m; $f_{(p,\mathrm{WW})} = 0.09$ Hz] [Note: There are different $H_{s,\mathrm{IG}}$ color scales in (a) and (b)]

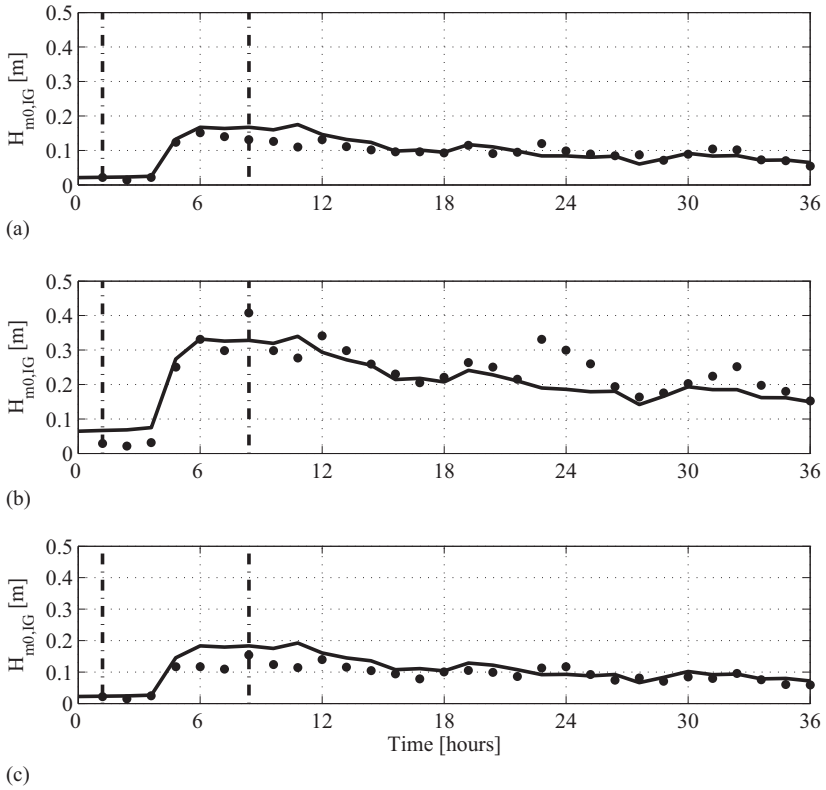

Fig. 13. Observed (black circles) and predicted (solid lines) infragravity significant wave height versus time at pressure Sensors (a) 1, (b) 5, and (c) 7

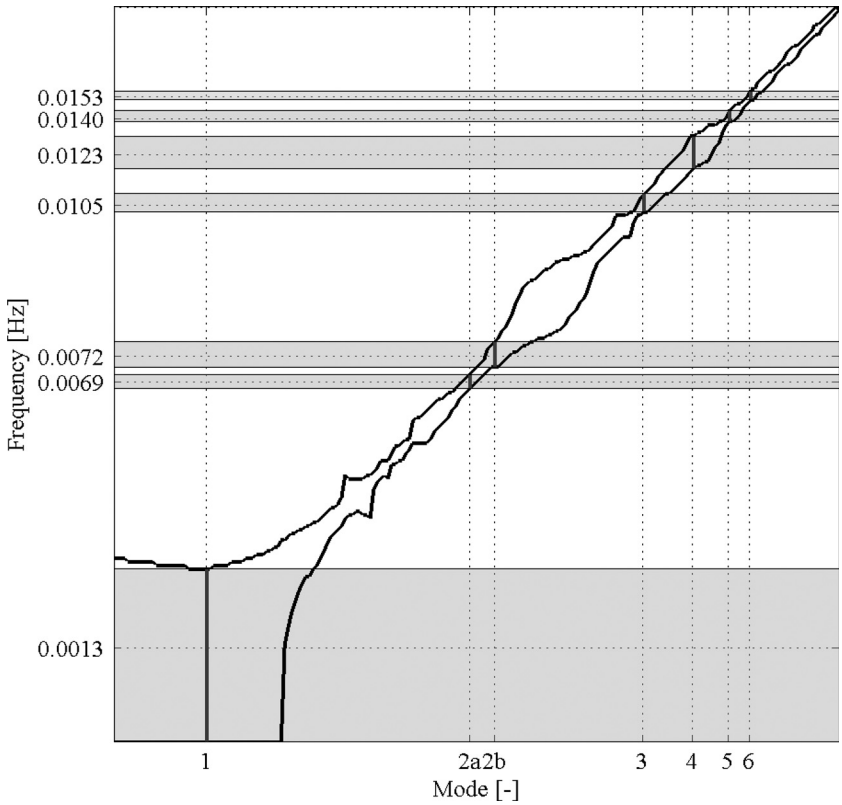

Fig. 14. Solid black lines correspond to MAC = 95%, and vertical solid lines show frequency band width considered for each mode

$\alpha E_{WW}^{\beta} f_{p,WW}^{\gamma}$ [Eq. (1)]. Best fits for α, β, and γ for each mode (Fig. 10 and Table 1) are the key empirical result. The similar β and γ of Modes 3–6 suggest similar excitation mechanisms.

Operational Model: Seiche Nowcast and Forecast

Given wind wave energy E_{WW} and peak frequency $f_{p,WW}$ outside the harbor, the seiche spectrum at any location within the harbor is given by $E'(\mathbf{x}, f_n)$, using the best fit harbor modal response parameters determined by fitting the entire 2 years' observations (Table 1). The observed evolution of harbor-averaged energy $E_{IG,IN}(f)$ is reproduced reasonably well in the hindcast, as shown for 36 h that included one of the most severe storms (Fig. 11).

Mode 1 is always the mode with the highest harbor-averaged energy $E_{IG,IN}(f)$, and is especially dominant with low-energy seas. In this case, most locations around the inner harbor quay wall have approximately equal seiche agitation ($H_{s,IG}$ between 0.04 and 0.06 m, Fig. 12, left). In contrast, during the most energetic storms, higher frequency energy high modes dominate at local hot spots with $H_{s,IG}$ up to 0.4 m (Fig. 12, right). The calibrated model skillfully reproduces $H_{s,IG}$ at a hot spot (P5) and at more typical locations (P1 and P7, Fig. 13).

Summary

A method is developed to predict seiche at infragravity periods in small harbors on ocean coasts from routinely available wind wave properties seaward of the harbor. The method, successfully applied at Marina di Carrara Harbor on the Mediterranean Sea, uses the mild-slope equations to establish the spatial structure of seiche modes and field observations to calibrate the response of each mode to the energy and peak frequency of wind waves seaward of the harbor. Predictions of infragravity seiche within the harbor compare well with the 2-year long calibration data set.

The approach appears well suited to small, shallow, steep-sided, coastal harbors that are sheltered from direct agitation by sea and swell, but is subject to low-frequency seiches. Previous observations at small harbors on Atlantic and Pacific shorelines are consistent with the forcing parametrization [Eq. (1)], and with preferentially excited normal modes with spatial structure given by the mild-slope type [Eq. (2)] [Bowers (1992); Okihiro and Guza (1996); and many others]. Guerrini et al. (2014) characterized seiche at Carrara with mild-slope spatial structure and a single set of amplitude parameters (α, β, and γ) for the most energetic 10% of the seiches. Here that approach is extended to all conditions by using a unique set of empirical parameters (α, β, and γ) for each of the most energetic six modes within the infragravity wave frequency bands. The nonlinear dynamics (e.g., energy losses through eddy formation) governing harbor response in energetic conditions are included empirically, yielding a realistic representation of the changes in mode mix with changing short wave conditions (Figs. 5 and 12). With limited modeling effort, this approach provides a quantitatively accurate representation of the variation of the long wave spectra within the harbor with changing incident wind wave conditions and locations along the harbor quays. With calibration and networked real-time sensors, a mode-resolving system can potentially provide a fast and accurate forecast of long wave elevations throughout the harbor.

The nonlinear coupling between seiche and wind waves is empirical, and the effect of variable incident wave direction is neglected. The model skill beyond conditions used in calibration, and at other harbors, is uncertain. Fluid velocities, critical for harbor operations, may be poorly modeled (Mei et al. 2005). In the future,

J. Waterway, Port, Coastal, Ocean Eng., 2017, 143(5): 04017032

improved phase-resolving, nonlinear models could include flow separation at sharp edges, time varying forcing, short wave breaking, and nonlinear interaction between seiche modes. Coupled with field measurements, these tools would provide further insight into the dynamic response of harbors.

Appendix. MAC

The MAC (Allemang 2003) is used to identify the frequency range, for each mode, over which the mode spatial shape is similar. The consistency between any two spatial structures (modal vectors) is defined as a scalar constant

$$\mathrm{MAC}_{\mathrm{cdr}} = \frac{|\{\psi_{\mathrm{cr}}\}^T \{\psi^*_{\mathrm{dr}}\}|^2}{\{\psi_{\mathrm{cr}}\}^T \{\psi^*_{\mathrm{cr}}\} \{\psi_{\mathrm{dr}}\}^T \{\psi^*_{\mathrm{dr}}\}} \tag{6}$$

where ψ_{cr} = modal coefficient for degree-of-freedom (DOF) c, mode r; ψ_{dr} = modal coefficient for DOF d, mode r; $\{\psi\}^T$ = transpose of ψ; and $\{\psi\}^*$ = complex conjugate of ψ.

The MAC varies between 0 (orthogonal spatial structures) and 1.0 (identical structures within a constant). The authors calculated MAC for all the η (complex surface elevation) that are a solution of Eq. (2) for frequencies in the range $0.0001 < f < 0.02$ Hz. For each of the resonant modes ($r = 1, 2a, 2b, 3, 4, 5, 6$), the bandwidths for which MAC > 0.95 are shown as vertical bold lines in Fig. 14. They correspond approximately to the observed band of high amplification in the harbor [shaded bands in Figs. 2(d and f)], and have been used to estimate the modal energy in a mode (e.g., Figs. 10–13).

Acknowledgments

Support for observations and analysis from the Port Authority of Marina di Carrara and HR Wallingford is gratefully acknowledged. Professor Guza was supported partially by the California Department of Parks and Recreation, Division of Boating and Waterways. Support from Dr. Ivano Melito (Port Authority of Marina di Carrara) and Dr. Alessandro Iannotta (API Nòva Energia) is warmly acknowledged.

References

Allemang, R. (2003). "The modal assurance criterion—Twenty years of use and abuse." *Sound Vib.*, 37(8), 14–23.

Bellotti, G., Briganti, R., Beltrami, G. M., and Franco, L. (2012). "Modal analysis of semi-enclosed basins." *Coastal Eng.*, 64(Jun), 16–25.

Belotti, G., and Franco, L. (2011). "Measurement of long waves at the harbor of Marina di Carrara, Italy." *Ocean Dyn.*, 61(12), 2051–2059.

Berkhoff, J. (1976). "Mathematical models for simple harmonic linear water waves: Wave diffraction and refraction." Ph.D. thesis, Delft Hydraulics Lab, Delft, Netherlands.

Bowers, E. (1992). "Low frequency waves in intermediate water depths." *Proc., 23rd Int. Conf. of Coastal Engineering*, 151, ASCE, Reston, VA, 832–845.

Briggs, M., Dykstra, D., and Baldwin, T. (2005). "Modeling of harbor resonance in Port of Long Beach." *Proc., Civil Engineering in the Oceans VI*, ASCE, Reston, VA, 479–493.

de Jong, M., and Battjes, J. (2004). "Seiche characteristics of Rotterdam Harbour." *Coastal Eng.*, 51(5–6), 373–386.

Gomis, D., Monserrat, S., and Tintoré, J. (1993). "Pressure-forced seiches of large amplitude in inlets of the Balearic Islands." *J. Geophys. Res. C: Oceans*, 98(C8), 14437–14445.

Graham, G., Chapman, D., Black, P., and Fornshell, J. A. (1990). "Causation of large-amplitude coastal seiches on the Caribbean coast of Puerto Rico." *J. Phys. Oceanogr.*, 20, 1449–1458.

Guerrini, M., Bellotti, G., Fan, Y., and Franco, L. (2014). "Numerical modelling of long waves amplification at Marina di Carrara harbour." *Appl. Ocean Res.*, 48(Oct), 322–330.

Hasselmann, K. (1962). "On the non-linear energy transfer in a gravity-wave spectrum." *J. Fluid Mech.*, 12(4), 481–500.

Herbers, T., Elgar, S., Guza, R., and O'Reilly, W. (1995). "Infragravity-frequency (0.005–0.05 Hz) motions on the shelf. Part II: Free waves." *J. Phys. Oceanogr.*, 25(6), 1063–1079.

Iannotta, A. (2002). "Development and application of a numerical model solving mild slope equation." M.Sc. thesis, Sapienza Univ. of Rome, Rome.

Ichinose, G., Anderson, J. G., Satake, K., Schweickert, R., and Lahren, M. (2000). "The potential hazard from tsunami and seiche waves generated by large earthquakes within Lake Tahoe, California-Nevada." *Geophys. Res. Lett.*, 27(8), 1203–1206.

Isobe, M., Kondo, K., and Horikawa, K. (1984). "Extension of MLM for estimating directional wave spectrum." *Proc., Symp. on Description and Modeling of Directional Seas*, Danish Hydraulic Institute, Hørsholm, Denmark, 15.

Lee, J., Lai, C., and Li, Y. (1998). "Application of computer modeling for harbor resonance studies of Long Beach and Los Angeles harbor basins." *Proc., 26th Int. Conf. on Coastal Engineering*, B. L. Edge, ed., ASCE, Reston, VA, 1196–1209.

Lepelletier, T. (1981). "Tsunamis–Harbor oscillations induced by nonlinear transient long waves." Ph.D. thesis, California Institute of Technology, Pasadena, CA.

Lepelletier, T., and Raichlen, F. (1987). "Harbor oscillations induced by nonlinear transient long waves." *J. Waterway, Port, Coastal, Ocean Eng.*, 10.1061/(ASCE)0733-950X(1987)113:4(381), 381–400.

Li, D. (2002). "Los Angeles-Long Beach Harbor Pier 400–Harbor resonance study using numerical model, CGWAVE." M.Sc. thesis, Univ. of Maine, Orono, ME.

Longuet-Higgins, M., and Stewart, R. (1960). "Changes in the form of short gravity waves on long waves and tidal currents." *J. Fluid Mech.*, 8(4), 565–583.

Losada, I., Gonzalez-Ondina, J., Diaz-Hernandez, G., and Gonzales, E. (2008). "Numerical modeling of nonlinear resonance of semi-enclosed water bodies: Description and experimental validation." *Coastal Eng.*, 55(1), 21–34.

Mei, C., Stiassnie, M., and Yue, D. (2005). *Theory and application of ocean surface waves*, World Scientific, Singapore, 23.

Melito, I., Cuomo, G., Bellotti, G., and Franco, L. (2006). "Field measurements of harbour resonance at Marina di Carrara." *Proc., 30th Int. Conf. on Coastal Engineering ICCE2006*, World Scientific, Singapore, 2, 1280–1292.

Melito, I., Cuomo, G., Franco, L., and Guza, R. (2007). "Harbour resonance at Marina di Carrara: Linear and non-linear aspects." *Proc., 5th Int. Conf. Coastal Structure 2007*, 2, 1647–1658.

Munk, W. (1949). "Surf beats." *Eos Trans. AGU*, 30, 849–854.

Okihiro, M., and Guza, R. (1996). "Observations of seiche forcing and amplification in three small harbors." *J. Waterway, Port, Coastal Ocean Eng.*, 10.1061/(ASCE)0733-950X(1996)122:5(232), 232–238.

Okihiro, M., Guza, R., and Seymour, R. (1992). "Bound infragravity waves." *J. Geophys. Res. Oceans*, 97(C7), 11453–11469.

Poon, Y., Raichlen, F., and Walker, J. (1998). "Application of physical model in long wave studies for the Port of Long Beach." *Proc., 26th ICCE*, Copenhagen, Denmark, 2, B. L. Edge, ed., ASCE, Reston, VA, 1222–1235.

Sand, S. (1982). "Wave grouping described by bounded long waves." *Ocean Eng.*, 9(6), 567–580.

Seabergh, W. (1993). "Analysis of prototype long period waves for Los Angeles/Long Beach Harbor resonance studies." *Proc., 2nd Int. Symp., Ocean Wave Measurement and Analysis*, ASCE, Reston, VA, 15–27.

Sobey, R. (2006). "Normal mode decomposition for identification of storm tide and tsunami hazard." *Coastal Eng.*, 53(2–3), 289–301.

Steward, D., and Panchang, V. (2001). "Improved coastal boundary condition for surface water waves." *Ocean Eng.*, 28(1), 139–157.

Stockdon, H., Holman, R., Howd, P., and Sallenger, A., Jr. (2006). "Empirical parameterization of setup, swash and runup." *Coastal Eng.*, 53(7), 573–588.

Thotagamuwage, D., and Pattiaratchi, C. (2013). "Numerical modelling of infra-gravity period oscillations in a marina." *Proc., 4th Int. Conf. on the Application of Physical Modelling to Port and Coastal Protection (Coastlab12)*, Dept. of Civil Engineering, Ghent Univ., Ghent, Belgium, 1, 514–523.

Vidal, C., Medina, R., Monserrat, S., and Martín, F.L. (2000). "Harbor resonance induced by pressure-forced surface waves." *Proc., 27th Int. Conf. of Coastal Engineering*, ASCE, Reston, VA, 3615–3628.

Woo, S., and Liu, P. (2004). "Finite-element model for modified Boussinesq equations. II: Applications to nonlinear harbor oscillations." *J. Waterway, Port, Coastal, Ocean Eng.*, 10.1061/(ASCE)0733-950X(2004)130:1(17), 17–28.